Super-resolution Processing of Multi-static Data Using Time Reversal and MUSIC

A.J. Devaney*
Department of Electrical Engineering
Northeastern University
Boston, MA 02115

Abstract

The problem of estimating the location of one or more coherent point scatterers from the *time-reversal matrix* as computed from backscattered narrow or broadband multi-static data is investigated. For the case of homogeneous backgrounds it is shown that under very weak conditions and as long as the number of sensor elements exceeds the number of scatterers the time reversal matrix has a rank equal to the number of scatterers so that the well-known vector subspace methods underlying the MUSIC algorithm can be applied to this matrix. A MUSIC type of algorithm is presented which computes a "pseudo-spectrum" of the location of M coherent point targets from multistatic data obtained using an N ($N > M$) element sensor array. The algorithm is tested in computer simulations and shown to yield excellent results, especially in the case of very sparse arrays where conventional time-reversal imaging breaks down.

1 Introduction

Two methodologies that have received considerable attention in the general area of array processing are *time-reversal imaging* [1, 2, 3, 4] and *MUSIC* (Standing for **MU**ltiple-**SI**gnal-**C**lassification) [5, 6] and related methods. In time-reversal imaging one or more unknown targets (scatterers) are sequentially probed using a set of N antennas[1] and the backscattered returns are measured at all the antenna locations yielding the so-called *multistatic response matrix* $K_{i,j}$, with i and j ranging from one to N. The multistatic response matrix is then used to compute the Hermitian *time-reversal-matrix* $T = K^{\dagger}K$ whose eigenvectors can be shown to correspond, in a one-to-one manner, with the different targets[2]. In particular, the wavefield generated from the array when excited by one of these eigenvectors focuses on the associated target so that if the Green function of the medium in which the targets are embedded (background medium) is known a synthetic image of the target locations is easily computed [1, 2, 4].

Subspace methods in statistical signal processing [5, 6] are also used for detecting and locating targets from antenna array data. However, these methods have, up to the present, been used in conjunction with the autocorrelation function (ACF) as computed from *passive* array data. Although these methods can be easily adapted to active arrays and, in particular, to *SAR imaging* (SAR standing for **S**ynthetic-**A**perture-**R**adar) they have serious limitations when multiple *coherent* targets are present or when sufficient data is not available for estimating the ACF. In particular,

*Support for this work was provided by Air Force Contracts # F41624-99-D6002 and # F49620-99-C0013

[1]We will use the term "antenna" to denote both acoustic as well as electromagnetic sensor elements in a phased array system.

[2]This statement is strictly true only if the targets are well-resolved (see discussion in section 2).

MUSIC fails completely for multiple targets and narrow band data unless the targets are uncorrelated. Although methods have been devised to deal with correlated targets [7, 8] they are generally difficult to apply and require wide-band data.

In this paper we will describe how subspace methods can also be used in conjunction with active phased array systems and, in particular, can be applied to the problem of locating M coherent point targets ($M < N$) from the measured $N \times N$ multi-static response matrix $K = K_{i,j}$ of the antenna array. In place of the ACF, which forms the basis for classical MUSIC, the scheme described here employs the $N \times N$ time-reversal matrix (TR matrix) $T = K^{\dagger}K$ whose eigenvectors play the role of the eigenvectors of the ACF in classical MUSIC. The rank of the TR matrix is investigated for the case of homogeneous backgrounds in three space dimensions R^3 and a theorem is proven that places severe restrictions on the geometrical distribution of targets in order for the rank of the TR matrix to be less than M. It then follows that when additive noise is present the N dimensional space of antenna voltages C^N can be partitioned into the direct sum of a *signal subspace* $\mathcal{S}$ and a *noise subspace* $\mathcal{N}$: $C^N = \mathcal{S} \bigoplus \mathcal{N}$ in complete analogy with classical MUSIC. A pseudo-spectrum is then computed using a steering vector equal to the background Green function (which models the antenna return from an isolated target at a "test" location). The pseudo-spectrum then yields super-resolved target locations in a manner completely analogous to the use of the pseudo-spectrum in resolving closely spaced spectral lines or closely spaced angles of arrival in classical MUSIC [5, 6]. Thus the coupling of time-reversal field processing with subspace methods, particularly with the MUSIC algorithm, lead to a powerful approach for detecting and locating targets in both homogeneous and non-homogeneous backgrounds especially in cases of closely spaced targets and/or very sparse antenna arrays as are employed, for example, in the *TechSat 21* program under consideration by the Air Force.

The paper employs a scalar wave formulation and, hence, is strictly applicable only to acoustic or ultrasound applications where the phased array system is an N element transducer array. However, the basic ingredients and conclusions of the theory apply equally well to electromagnetic fields where the phased array system is an N element antenna array and, indeed, we will use the term "antenna" to encompass both acoustic as well as electromagnetic array elements and will not make a distinction between these two types of applications in the paper. The paper is directed primarily at *near field* target detection and location estimation where the target separation is sufficient where multiple scattering between different targets can be ignored and the Born approximation used. Although the underlying ideas and mathematics are easily generalized to medium and far field problems such as occur with air and satellite surveillance the generalization to take into account multiple scattering between different targets is not simple although it can, in principle, be included in the theory [3]. Also the theory is developed entirely in the frequency domain and so applies equally to narrow band or broad band antenna elements. Finally, it should be mentioned that although the theory is developed for point scatterers and ideal point (monopole) antenna elements the generalization to continuously distributed targets and realistic antennas and to the full electromagnetic (vector fields) case is not difficult and is currently under development.

2 Mathematical Model

Throughout this paper we will work entirely in the frequency domain. Thus, we tacitly assume that the time-dependent signals are expressible in the Fourier integral

$$X(t) = \frac{1}{2\pi} \int_{-\infty}^{\infty} d\omega \, \tilde{X}(\omega) e^{-i\omega t}$$

with

$$\tilde{X}(\omega) = \int_{-\infty}^{\infty} dt \, X(t) e^{i\omega t}.$$

Within the frequency domain and for *real valued* time-dependent signals, time-reversal becomes phase conjugation as is easily verified from the above Fourier transform relations. *Thus, from this point on the time-reversal operation will be synonymous with phase conjugation in the frequency domain.*

We consider an array of N antennas, centered at the space points $\mathbf{R}_j$, $j = 1, 2, \ldots, N$. We make no assumptions about the location of the antenna elements and, in particular, do not require them to lie in a plane or be requlary spaced. Each antenna is assumed to radiate a scalar field $\psi_j(\mathbf{r}, \omega)$ into a half-space $z > 0$ in which are embedded one or more scatterers (targets). Within this paper we make the simplifying assumptions that the antennas are monopoles (point antennas) and the targets are ideal point scatterers and, in addition, neglect all multiple scattering between targets. Under these assumptions the wavefield radiated by the j'th antenna element and the resulting scattered field are equal to

$$\psi_j(\mathbf{r}, \omega) = G(\mathbf{r}, \mathbf{R}_j) e_j(\omega) \tag{1}$$

$$\psi_j^{(s)}(\mathbf{r}, \omega) = \sum_{m=1}^{M} G(\mathbf{r}, \mathbf{X}_m) \tau_m(\omega) G(\mathbf{X}_m, \mathbf{R}_j) e_j(\omega) \tag{2}$$

where the sum is over all the targets and $\tau_m(\omega)$ is the target scattering amplitude and $\mathbf{X}_m$ is the location of the m'th target. Here, $e_j(\omega)$ is the input voltage applied at the terminals of the j'th antenna element, $G(\mathbf{r}, \mathbf{r}')$ is the Green function of the medium in which the targets are embedded (background medium) and ω is the frequency. When all antenna elements are simultaneously excited using the voltages e_j, $j = 1, 2, \ldots, N$ then the total incident and scattered wavefields are given by

$$\psi(\mathbf{r}, \omega) = \sum_{j=1}^{N} \psi_j = \sum_{j=1}^{N} G(\mathbf{r}, \mathbf{R}_j) e_j(\omega) \tag{3}$$

$$\psi^{(s)}(\mathbf{r}, \omega) = \sum_{j=1}^{N} \psi_j^{(s)} = \sum_{j=1}^{N} \sum_{m=1}^{M} G(\mathbf{r}, \mathbf{X}_m) \tau_m(\omega) G(\mathbf{X}_m, \mathbf{R}_j) e_j(\omega). \tag{4}$$

The voltage output $v_l(\omega)$ from the l'th antenna is assumed to be equal to the amplitude of the scattered field as measured at the l'th antenna and is then given by

$$\begin{aligned} v_l(\omega) &= \sum_{j=1}^{N} \psi_j^{(s)}(\mathbf{R}_l, \omega) \\ &= \sum_{j=1}^{N} \sum_{m=1}^{M} G(\mathbf{R}_l, \mathbf{X}_m) \tau_m(\omega) G(\mathbf{X}_m, \mathbf{R}_j) e_j(\omega). \end{aligned} \tag{5}$$

We can express the above equations in a compact matrix notation by introducing the N dimensional "Green function" column vectors $g_m(\omega)$:

$$g_m(\omega) = \{G(\mathbf{R}_l, \mathbf{X}_m)\} = [G(\mathbf{R}_1, \mathbf{X}_m), G(\mathbf{R}_2, \mathbf{X}_m), \ldots, G(\mathbf{R}_N, \mathbf{X}_m)]^T. \tag{6}$$

In terms of these column vectors we define the symmetric *multi-static response matrix* (MSR matrix)

$$K = \{K_{l,j}\} = \sum_{m=1}^{M} G(\mathbf{R}_l, \mathbf{X}_m) \tau_m(\omega) G(\mathbf{X}_m, \mathbf{R}_j) = \sum_{m=1}^{M} \tau_m g_m g_m^T \tag{7}$$

where we have suppressed displaying the explicit dependence of the scattering coefficient and Green function vectors on frequency. In terms of the MSR matrix we can write Eq.(5) in the form

$$v_l = \sum_{j=1}^{N} K_{l,j} e_j = Ke$$

where $e = \{e_j\} = [e_1, e_2, \ldots, e_N]^T$ is the N-dimensional column vector formed from the set of input voltages applied at the antenna terminals.

We conclude this section by noting that the Green functions $G(\mathbf{r}, \mathbf{r}')$ are completely general in the sense that the above formulation applies to both homogeneous and non-homogeneous media, including media with boundaries and highly dispersive media. Of course some of the computations to be performed later will require that these Green functions be known and that will limit the generality of the formulation in practice. However, two important cases where the Green functions can be easily computed are:

- Homogeneous dispersive and non-dispersive media,
- Parallel layered media including a half-space with a planar interface.

The examples that we present later are for homogeneous media at a single frequency but can be trivially extended to both of the above cases.

3 Time reversal matrix

We define the *time-reversal matrix* T to be

$$T = K^{\dagger} K = K^* K \tag{8}$$

where the superscript † denotes the adjoint matrix and where the second equality follows from the fact that the multi-static response matrix is symmetric so that $K^{\dagger} = K^*$ where the superscript asterisk * denotes the complex conjugate. In terms of the green function vectors we conclude using Eq.(7) that

$$\begin{aligned} T &= [\sum_{m=1}^{M} \tau_m g_m g_m^T]^* [\sum_{m'=1}^{M} \tau_{m'} g_{m'} g_{m'}^T \\ &= \sum_{m=1}^{M} \sum_{m'=1}^{M} \Lambda_{m,m'} g_m^* g_{m'}^T \end{aligned} \tag{9}$$

where

$$\Lambda_{m,m'} = \tau_m^* \tau_{m'} < g_m, g_{m'} > \tag{10}$$

where the angular brackets stand for the standard inner product in C^N; i.e.,

$$< g_m, g_{m'} >= g_m^{\dagger} g_{m'} = \sum_{n=1}^{N} g_m^*(n) g_{m'}(n).$$

3.1 Rank of the time-reversal matrix

The rank of the time-reversal matrix T is the same as the rank of the MSR matrix K and is a quantity that will be important in the material to follow. Since K is, by its definition Eq.(7), a linear sum of outer product matricies formed from the Green function vectors g_m, $m = 1, 2, \ldots, M$, its rank will be equal to the number of these vectors that are linearly independent. For the special case of a homogeneous background and three space dimensions we have the following theorem which is proved in the appendix

Theorem 1 *The time-reversal matrix T for an N element array embedded in a three-dimensional homogeneous background having wavenumber k with $\Im k > 0$ and containing $1 < M \leq N$ targets will have rank $< M$ if and only if the following conditions hold:*

1. *All of the targets are located on a single plane $\mathcal{P}$ that is orthogonal to at least $N - M + 1$ lines $l_{j,l}$ connecting different antenna elements labeled by indicies j and l,*

2. *The plane $\mathcal{P}$ is the perpendicular bisector of the $N - M + 1$ lines satisfying condition (1) or all targets on $\mathcal{P}$ are equidistant from every line satisfying condition (1).*

The above theorem places severe restrictions on the geometrical distribution of targets in order for the rank of the time-reversal matrix to be less than the number of targets. Indeed, condition 1 by itself is very restrictive, especially for non-linear or non-planar arrays. For example if the antenna array is not linear or planar then condition 1 cannot be realized if the number of antenna elements $N > 3$. This follows from the fact that three or more non-parallel planes can intersect in no more than a single point. For linear arrays Condition 2 requires that all the targets be located equidistant to the line of the array. Although configurations of targets exist that will all lie on a single plane that is perpendicular to the line of the array *and*, be equidistant from this line, it is clear that such configurations are very special and unlikely to be encountered in any given experiment.

A few additional comments are in order as regards the above theorem. First, the requirement that there be at least some absorbtion ($\Im k > 0$) is required in order to eliminate additional, very special target geometries that can reduce the rank of the MSR matrix (see discussion in the appendix). Thus, the theorem will still hold for purely non-absorbing backgrounds except for certain special target geometries. Also, the theorem says nothing about the magnitude of the eigenvalues of the time-reversal matrix. In particular, certain eigenvalues may become very small in certain situations. For example, if two or more target locations $\mathbf{X}_m$ become close relative to a wavelength we can expect that the associated Green function vectors will become nearly parallel (in C^N) so that the *effective* rank of the time-reversal matrix will be reduced. We will return to this point later when we present simulations showing that the effective rank of T is, in general, reduced for closely spaced targets. However, this issue is somewhat moot within the context of the present paper since we have ignored multiple scattering between targets so that our results only apply to well separated targets.

We conclude this section by noting that Theorem 1 also holds in the case of homogeneous backgrounds in two-space dimensions R^2 under the usual asymptotic approximation

$$G(\mathbf{R}, \mathbf{X}) = \frac{-i}{4} H_0(k|\mathbf{R} - \mathbf{X}|) \sim -\sqrt{\frac{1}{8\pi k}} \frac{e^{ik|\mathbf{R}-\mathbf{X}|}}{\sqrt{|\mathbf{R} - \mathbf{X}|}} \tag{11}$$

where H_0 is the zero order Hankel function of the first kind. The approximation in the above equation is accurate so long as the distance between the antenna location $\mathbf{R}$ and the target location $\mathbf{X}$ exceeds about three wavelengths. The case of two space dimensions corresponds physically to where the antennas are line sources and the targets line scatterers all perpendicular to the plane R^2. From a purely mathematical point-of-view one can just as well consider the antenna elements and the scatterers as simply points in the two-dimensional space R^2. We will take this latter view in the following discussion. It is easily verified that the steps used in proving Theorem 1 (see appendix) for R^3 also hold in R^2 under the above approximation to the Green function. For the case of R^2 where all antenna elements and targets are points in a single plane condition 1 of Theorem 1 requires that all the targets lie on a straight line that is perpendicular to $N-M+1$ lines connecting different antenna elements. This condition cannot be satisfied if $M < N$ for non-linear arrays while condition 2 cannot be satisfied for linear arrays if $M < N$ if we also require all the targets to lie in the same half-space relative to the linear array. In the simulations that we will present later we use two-space dimensions and all of the targets will be located in a single half-space relative to the antenna array elements so that the rank of the time-reversal matrix will be guaranteed to be M so long as $M < N$.

3.2 Eigenvalues and Eigenvectors of the Time-reversal matrix

The time reversal matrix T is Hermitian ($T^\dagger = T$) and non-negative ($< v, Tv > \geq 0$, $\forall v \in C^N$). Because of these facts the matrix possesses a complete set of orthonormal eigenvectors having non-negative eigenvalues. As we have just shown in Theorem 1 under very weak conditions and for the case of homogeneous backgrounds with $\Im k > 0$ the rank of this matrix will be equal to M, the number of targets, if $M \leq N$ and will be N, the number of antennas, if $M > N$. We will from this point on simply assume that $M \leq N$ and the rank of T is equal to M so that there are exactly M non-zero eigenvalues. We distinguish two cases corresponding to *well resolved targets* and *non-well resolved targets*.

3.2.1 Well resolved targets

We first consider the case of *well-resolved targets* which is defined to be the case where the quantity $\Lambda_{m,m'}$ defined in Eq.(10) is approximately zero when $m \neq m'$. This occurs when the Green function vectors form an (approximate) orthogonal set or, equivalently, when the inner product between two different Green function vectors is approximately zero; i.e.,

$$< g_m, g_{m'} >= \sum_{n=1}^{N} g_m^*(n) g_{m'}(n) = \sum_{n=1}^{N} G^*(\mathbf{R}_n, \mathbf{X}_m) G(\mathbf{R}_n, \mathbf{X}_{m'}) \approx 0, \tag{12}$$

for $m \neq m'$. We can interpret the quantity

$$H(\mathbf{r}, \mathbf{X}_{m'}) = \sum_{n=1}^{N} G^*(\mathbf{R}_n, \mathbf{r}) G(\mathbf{R}_n, \mathbf{X}_{m'}) \tag{13}$$

as being the *coherent point spread function (CPSF) of the antenna array*. In particular, this quantity represents an "image" of the source point $\mathbf{X}_{m'}$ formed by the antenna array from measurement of the outgoing wave Green function $G(\mathbf{r}, \mathbf{X}_{m'})$ at the various array elements; i.e., for $\mathbf{r} = \mathbf{R}_n$, $n = 1, 2, \ldots, N$. Mathematically this equation represents the CPSF in terms of the *backpropagation* of the outgoing wave Green function $G(\mathbf{r}, \mathbf{X}_{m'})$ from the antenna array into the half-space $z > 0$. It follows that the inner product $< g_m, g_{m'} >$ defined in Eq.(12) is the antenna array point spread function evaluated at the image point $\mathbf{r} = \mathbf{X}_m$ and the quantity Λ defined in Eq.(10) can be expressed in terms of the CPSF as

$$\Lambda_{m,m'} = \tau_m^* \tau_{m'} H(\mathbf{X}_m, \mathbf{X}_{m'}) \tag{14}$$

For large, closely spaced, regular arrays the CPSF will have a maximum at the source point location $\mathbf{r} = \mathbf{X}_{m'}$ and will decay in amplitude for points removed from this image point. For sparse arrays or for arrays having few elements the CPSF will have a complicated structure that consists of ridges and valleys that converge to the source point at which the CPSF achieves a local maximum or, at least, a maximum in some plane or line that contains the source point. The effective spatial extent of the point spread function is determined by the geometry of the antenna array and the wavelength of the radiation. For example, for a densely spaced (less than a half-wavelength spacing) square antenna array, the *transverse* effective spatial region of support of the CPSF is roughly a square having sides of length $z\lambda/a$ where z is the distance from the array, $a = N\delta$ is the length of the side of the array with δ being the spacing between array elements. The extent of the region of the CPSF in the longitudinal direction (z direction) is considerably larger and, again, depends on the wavelength and array geometry. We conclude from the above discussion that if the two target locations $\mathbf{X}_m$ and $\mathbf{X}_{m'}$ are separated by a distance larger than the effective spatial extent of the CPSF then $\Lambda_{m,m'}$ reduces approximately to

$$\Lambda_{m,m'} = |\tau_m|^2 \rho_m \delta_{m,m'} \tag{15}$$

where

$$\rho_m = H(\mathbf{X}_m, \mathbf{X}_m) =< g_m, g_m > \tag{16}$$

is the squared norm of the m'th Green function vector and $\delta_{m,m'}$ is the Kroneka delta function. This is the case of well-resolved targets.

By making use of Eq.(15) we find using Eq.(9) that the time-reversal operator assumes the simple form

$$T = \sum_{m=1}^{M} |\tau_m|^2 \rho_m g_m^* g_m^T. \tag{17}$$

which is recognized as a *projection operator onto the subspace spanned by the complex conjugates of the Green function vectors* g_m. Moreover, since for the well-resolved case, the Green function vectors are orthogonal with norm squared equal to ρ_m; i.e.,

$$< g_m, g_{m'} >= \rho_m \delta_{m,m'}$$

we conclude that eigenvectors of the time-reversal matrix in this case are precisely the complex conjugate of the Green function vectors and the eigenvalues are equal to $|\tau_m|^2|\rho_m|^2$; i.e.,

$$\begin{aligned} T g_{m_0}^* &= \sum_{m=1}^{M} |\tau_m|^2 \rho_m g_m^* g_m^T g_{m_0}^* \\ &= \sum_{m=1}^{M} |\tau_m|^2 \rho_m g_m^* \rho_{m_0} \delta_{m,m_0} \\ &= |\tau_{m_0}|^2 |\rho_{m_0}|^2 g_{m_0}^*. \end{aligned}$$

The complex conjugate of the Green function vectors comprise M eigenvectors of the time-reversal matrix which has dimension N^2 and, hence, possesses a total of N (orthogonal) eigenvectors. Under the assumption that the number of targets M is less than the number of antenna elements N, the remaining $N - M$ eigenvectors will have zero eigenvalues since they must be orthogonal to the Green function vectors; i.e.,

$$T\mu = \sum_{m=1}^{M} |\tau_m|^2 \rho_m g_m^* \overbrace{g_m^T \mu}^{<g_m^*, \mu>} = 0$$

where μ is an eigenvector in the orthogonal complement of the space spanned by the Green function vectors. For later purposes we will refer to the space spanned by the Green function vectors as the *signal subspace* and its orthogonal complement spanned by eigenvectors with zero eigenvalues as the *noise subspace*. Thus

$$C^N = \mathcal{S} \bigoplus \mathcal{N} \tag{18}$$

where $\mathcal{S} = \{\text{span}(g_m*, m = 1, 2, \ldots, M)\}$ is the signal subspace and $\mathcal{N}$ the noise subspace and where C^N is the space of N-dimensional complex valued column vectors (the space of applied voltages to the N element antenna array). Again, as indicated above, we tacitly assume that the number of targets is less than the number of antenna elements N.

3.2.2 Non-resolved targets

In the general case $\Lambda_{m,m'}$ will not be a diagonal matrix and the time-reversal matrix does not simplify from its general form given in Eq.(9); i.e.,

$$T = \sum_{m=1}^{M} \sum_{m'=1}^{M} \Lambda_{m,m'} g_m^* g_{m'}^T. \tag{19}$$

In this case we see that the time-reversal matrix is *still a projection operator onto the subspace spanned by the complex conjugates of the Green function vectors g_m (the signal subspace $\mathcal{S}$).* However, the eigenvectors of T are no longer simply the complex conjugates of the Green function vectors but, rather, will be linear superpositions of these vectors. Nevertheless, the decomposition of C^N into a direct sum of the signal and noise subspaces according to Eq.(18) still holds. Most importantly, we conclude from Theorem 1 *that the rank of T and, hence, the dimension of the signal subspace $\mathcal{S}$ remains equal to M* except for very specialized and unlikely target configurations.

For future reference we will denote the orthonormal set of eigenvectors of T by μ_m, $m = 1, 2, \ldots, M, M+1, \ldots, N$ where the first M of these eigenvectors have non-zero eigenvalues and span the signal subspace $\mathcal{S}$ and the remaining $N - M$ vectors have zero eigenvalues and span the noise subspace $\mathcal{N}$; i.e.,

$$\begin{aligned} T\mu_m &= \lambda_m \mu_m, \quad m = 1, 2, \ldots, M, \\ T\mu_m &= 0 \quad , \quad m = M+1, M+2, \ldots, N, \\ < \mu_m, \mu_{m'} > &= \delta_{m,m'}. \end{aligned}$$

We note that in the special case of well-resolved targets the normalized signal space eigenvectors are proportional to the complex conjugate of the Green function vectors:

$$\mu_m = \frac{g_m^*}{\sqrt{\rho_m}}, \quad m = 1, 2, \ldots, M. \tag{20}$$

We also define the projection operators onto the signal and noise subspaces, viz.,

$$P_{\mathcal{S}} = \sum_{m=1}^{M} \mu_m \mu_m^\dagger \tag{21}$$

$$P_{\mathcal{N}} = \sum_{m=M+1}^{N} \mu_m \mu_m^\dagger. \tag{22}$$

Since, C^N is the direct sum of the signal and noise subspaces (cf., Eq.(18)), the sum of the noise and signal space projection operators is equal to the identity operator in C^N:

$$P_{\mathcal{N}} + P_{\mathcal{S}} = I. \tag{23}$$

4 Focusing with the Time-Reversal Eigenvectors

The natural question arises as to how one makes use of the time-reversal matrix and, in particular, of the computed eigenvalues and eigenvectors to locate targets. The standard method that is used is simple imaging; i.e., one computes the image corresponding to each one of the different eigenvectors having non-zero eigenvalue and associates that image with one or some collection of the targets. We consider first the case of well resolved targets where the signal space eigenvectors of the time-reversal matrix are proportional to the complex conjugates of the Green function vectors $g_m^* = \{G^*(\mathbf{R}_j, \mathbf{X}_m)\}^T = \{G^*(\mathbf{X}_m, \mathbf{R}_j,)\}^T$ (cf., Eq.(20)). Consider now the radiated wavefield from the antenna array when the input voltage $e = \{e_j\}$ is equal to one of these signal space eigenvectors $\mu_m = \{\mu_m(j)\}$, $\quad m = 1, 2, \ldots, M$. From Eq.(3) we find that

$$\psi_m(\mathbf{r}, \omega) = \sum_{j=1}^{N} G(\mathbf{r}, \mathbf{R}_j) \mu_m(j) \tag{24}$$

$$= \frac{1}{\sqrt{\rho_m}} \sum_{j=1}^{N} G^*(\mathbf{X}_m, \mathbf{R}_j) G(\mathbf{r}, \mathbf{R}_j)$$
$$= \frac{1}{\sqrt{\rho_m}} H^*(\mathbf{r}, \mathbf{X}_m)$$

where we have made use of Eq.(20) and the definition of g_m^* and where $H(\mathbf{r}, \mathbf{X}_m)$ is the CPSF of the antenna array defined in Eq.(13). As discussed in Section 3.2.1 the CPSF is an "image" of the target point $\mathbf{X}_m$ formed by the phased array antenna. In other words, in the case of well resolved targets, *the wavefields radiated from applied voltage distributions equal to signal space eigenvectors focus at the target locations.* Thus, in the case of well-resolved targets it is only necessary to compute the image field using Eq.(24) and the target is located at the maximum value of the magnitude of this image.

It is important to note that in order to make use of Eq.(24) it is necessary to know (i.e., have an analytic or computer model) of the background Green function. Thus, although *computation of the eigevalues and eigenvectors of the time-reversal matrix requires no knowledge of the background, computation of the image field requires knowledge of the background Green function.* It is also important to note that the quality of the time-reversed images as computed using Eq.(24) depends critically on the number of array elements and the array geometry and will suffer serious degradation in some cases such as in the case of sparse arrays. As was discussed in section 3.2.1 the CPSF depends critically on array size, geometry and wavelength and, in particular, will exhibit pronounced side-lobes if the array is sparse. In such cases the image generated by the eigenvector may not peak at the actual target location and/or will have a number of local maxima. We will discuss how this impacts the target location problem and how the use of vector sub-space methods and, in particular, MUSIC can be used to circumvent many of these limitations later in the paper.

The above result does not, unfortunately, generalize to the case of non-resolved targets. In particular, for this more general case, the signal space eigenvectors are linear combinations of the complex conjugates of the Green function vectors. Thus, an applied voltage equal to one of these eigenvectors generates a linear combination of CPSF's, each focused on a different target location and each having a different amplitude. Since the targets are not resolved these image fields would interfere with each other so that the quality of the target location estimates would suffer. Because of this the use of focusing to locate and identify non-resolved targets is limited. However, as happens when the antenna arrays are sparse, vector sub-space methods such as MUSIC can be used in these more general situations as will be discussed below.

5 MUSIC

Our goal is to estimate the locations of the targets from the scattered field data. One approach to this goal is to employ the subspace methods used in signal classification and discrete spectrum estimation for this purpose. We describe in this section one such method called *MUSIC* (for "MUltiple-SIgnal-Classification"). We emphasize that the MUSIC algorithm is to be used *in conjunction* with time-reversal processing and not *in replacement* of time-reversal processing. Thus, we still will require multi-static data and the multi-static response matrix K and will compute the time-reversal matrix $T = K^*K$ and the eigenvalues and eigenvectors of this matrix. What we propose is *to replace the classical image formation process described in the previous section with the MUSIC scheme.* By doing this we will be able to deal both with non-resolved targets as well as with sparse antenna arrays, two cases where classical imaging fails.

The MUSIC algorithm makes use of the fact that the time-reversal matrix T is a projection operator onto the subspace of C^N spanned by the complex conjugates of the Green function vectors

(the *signal subspace*) and that the noise subspace $\mathcal{N}$ is spanned by the eigenvectors of T having zero eigenvalue. It then follows that *the complex conjugate of each Green function vector must be orthogonal to the noise subspace and, in particular, to the eigenvectors of the time-reversal matrix having zero eigenvalue*; i.e.,

$$< \mu_{m_0}, g_m^* >=< \mu_{m_0}^*, g_m > 0 \tag{25}$$

for $m = 1, 2, \ldots, M$, $m_0 = M+1, \ldots, N$, where μ_{m_0} are the eigenvectors of T having zero eigenvalue. We can then form a *pseudo-spectrum* according to the algorithm

$$D(\mathbf{X}_p) = \frac{1}{\sum_{m_0=M+1}^{N} | < \mu_{m_0}^*, g_p > |^2} \tag{26}$$

where μ_{m_0} is the m_0'th eigenvector of T having zero eigenvalue and

$$g_p(\omega) = \{G(\mathbf{R}_l, \mathbf{X}_p)\} = [G(\mathbf{R}_1, \mathbf{X}_p), G(\mathbf{R}_2, \mathbf{X}_p), \ldots, G(\mathbf{R}_N, \mathbf{X}_p)]^T \tag{27}$$

is the *steering vector*. The steering vector is seen to be the Green function vector for a target located at the *test location* $\mathbf{X}_p$. Because the signal subspace is orthogonal to the noise subspace the inner product $< \mu_{m_0}^*, g_p > |^2$, with $m_0 = M+1, \ldots, N$, will vanish when ever the test location $\mathbf{X}_p$ is equal to the actual location of one of the targets $\mathbf{X}_m$ and this will happen *for non-resolved targets as well as well-resolved targets*. We see from Eq.(26) that the pseudo-spectrum D will then peak (theoretically to infinity) at each target location; i.e., when $\mathbf{X}_p = \mathbf{X}_m$, $m = 1, 2, \ldots, M$. Eq.(26) is the MUSIC algorithm for time-reversal imaging.

5.1 Implementation of MUSIC

The denominator of the pseudo-spectrum Eq.(26) is simply the magnitude square of the projection of the complex conjugate of the steering vector onto the noise subspace. To perform this projection operation we can use the noise subspace projection operator defined in Eq.(22) or, equivalently, we can use represent this projection operator in terms of the signal subspace projection operator using Eq.(23). Thus, in particular, we have that

$$\sum_{m_0=M+1}^{N} | < \mu_{m_0}^*, g_p > |^2 = \sum_{m_0=M+1}^{N} | < \mu_{m_0}, g_p^* > |^2 = |P_{\mathcal{N}} g_p^*|^2 = |[I - P_{\mathcal{S}}] g_p^*|^2. \tag{28}$$

The two different methods of computing the pseudo-spectrum have different implementation implications. In particular, for large arrays and small number of targets the noise subspace is much larger than the signal subspace and there is thus an advantage of employing the signal space projection operator since there are fewer eigenvectors to compute. In the other extreme where the number of targets approaches the number of antenna elements the noise subspace has small dimension and it is advantageous to employ the noise space projection operator.

5.2 Connection with classical time-reversal imaging

The classical time-reversal image generated from an eigenvector μ_{m_0} in accordance with Eq.(24) can be expressed in the form

$$\psi_{m_0}(\mathbf{X}_p, \omega) = \sum_{j=1}^{N} G(\mathbf{X}_p, \mathbf{R}_j) \mu_{m_0}(j) =< \mu_{m_0}^*, g_p > \tag{29}$$

where we have replaced the field point $\mathbf{r}$ by $\mathbf{X}_p$ and where g_p is the Green function vector evaluated at $\mathbf{X}_p$ and defined in Eq.(27) and where μ_{m_0} is the m_0'th eigenvector of T having zero eigenvalue.

On making use of the above expression we can express the pseudo-spectrum defined in Eq.(26) in the form

$$D(\mathbf{X}_p) = \frac{1}{\sum_{m_0=M+1}^{N} |\psi_{m_0}(\mathbf{X}_p, \omega)|^2} \tag{30}$$

We can interpret Eq.(30) as stating that *the pseudo-spectrum is inversely proportional to the sum of the intensities (magnitude squares) of the images formed from the eigenvectors having zero eigenvalue.* Thus, the pseudo-spectrum can be computed from classically formed time-reversal images but *from the images corresponding to zero eigenvalue as opposed to the usually used non-zero eigenvalue.*

An alternative interpretation of the pseudo-spectrum can be obtained by making use of the alternative form of the projection operator onto the noise space $\mathcal{N}$. In particular, on making use of Eqs.(refeq:17), (21) and (29) we conclude that

$$\begin{aligned} \sum_{m_0=M+1}^{N} | < \mu_{m_0}, g_p^* > |^2 &= |[I - P_{\mathcal{S}}]g_p^*|^2 \\ &= |g_p^* - \sum_{m=1}^{M} \mu_m < \mu_m, g_p^* > |^2 \\ &= |g_p|^2 - \sum_{m=1}^{M} |\psi_m(\mathbf{X}_p, \omega)|^2. \end{aligned} \tag{31}$$

We can interpret Eq.(31) as stating that *the pseudo-spectrum is inversely proportional to the difference between the intensity of the image of the steering vector and the sum of the intensities of the images formed from the eigenvectors having non-zero eigenvalue.* Thus, the pseudo-spectrum can also be computed from classically formed time-reversal images corresponding to non-zero eigenvalues.

6 Matlab Computer Simulation

The time-reversal imaging and time-reversal-MUSIC estimation methods outlined above were tested in a simple computer simulation using MATLAB. The program assumes a two-dimensional geometry where the antenna elements are line sources and the targets are line targets all embedded in a homogeneous background and perpendicular to a single plane and all multiple scattering is ignored. As discussed earlier, from a mathematical point of view we can consider the targets and antenna elements as points in the two-dimensional space of the plane; i.e., as point locations in R^2. We will take this latter view in the discussion that follows.

In the R^2 case the appropriate Green function $G(\mathbf{r}, \mathbf{r}')$ is given in Eq.(11). The Green function vectors are then given by

$$g_m(\omega) = \{H_0(k|\mathbf{R}_l - \mathbf{X}_m|)\} = [H_0(k|\mathbf{R}_1 - \mathbf{X}_m|), H_0(k|\mathbf{R}_2 - \mathbf{X}_m|), \ldots, H_0(k|\mathbf{R}_N - \mathbf{X}_m|)]^T, \tag{32}$$

where we have dropped the unessential constant $-i/4$.

In the simulations we employed a basic image space which is a rectangular grid representing a section of the x, z plane with z being depth (pointing down) and x lateral location (with positive x directed to the right). All dimensions are in relative to the wavelength which is taken to be unity. The simulations used an image grid spacing parameter $\delta x = \delta z$ equal to a quarter wavelength $\delta x = \lambda/4$ and an equally spaced linear array of from five to nine elements (depending on the simulation) located at $z = 0$ and with adjacent antenna element spacing varying from a half-wavelength to up to sixteen wavelengths again depending on the simulation. We also used from

two to four targets located at the same z (depth) coordinate (sixteen wavelengths) but with variable spacing along the x direction. In some of the simulations we added additive white Gaussian noise (AWGN) to the computed MSR matrix K according to the model

$$\mathcal{K} = K + Ae^{i2\pi W} \tag{33}$$

where $\mathcal{K}$ is the noisy MSR matrix, A is an independent Gaussian variable with variance proportional to the peak amplitude of the ideal (computed) MSR matrix K and W an independent Gaussian variable with unit variance. All parameters used in any given example are listed in the figure captions.

6.0.1 Computing the Multi-static Response Matrix

The incident wave generated by the antenna array when excited by a unit amplitude voltage $e_{j'}(\omega) = \delta_{j,j'}$, $j' = 1, \ldots, N$ is from Eq.(1)

$$\psi_j(\mathbf{r}, \omega) = G(\mathbf{r}, \mathbf{R}_j) = H_0(k|\mathbf{r} - \mathbf{R}_j|)$$

$j = 1, 2, \ldots, N$ and where $\mathbf{r}$ can be the coordinate vector of any point in the basic image grid. In particular, the strength of the incident wave at the m'th target location is obtained by taking $\mathbf{r} = \mathbf{X}_m$. In the absence of multiple scattering and assuming a perfect delta function target the corresponding scattered field is defined by Eq.(2) with the amplitude $e_j = 1$ and with the field point $\mathbf{r} = \mathbf{R}_i$. We then obtain the MSR matrix $K = K_{i,j}$:

$$K_{i,j} = \psi_j^{(s)}(\mathbf{R}_i, \omega) = \sum_{m=1}^{M} G(\mathbf{R}_i, \mathbf{X}_m)\tau_m(\omega)G(\mathbf{X}_m, \mathbf{R}_j) \tag{34}$$

where τ_m are the scatterer strengths.

As an initial example we computed the MSR matrix using Eq.(34) for the case of two targets ($M = 2$) both located at a depth of sixteen wavelengths for a linear antenna array of nine elements that was centered over the image grid. In this first simulation we used a half-wavelength spacing for the antenna elements, no additive noise, and a target separation of eight wavelengths along the x direction, with one target located exactly at the mid-point of the array and the other displaced by eight wavelengths in the positive x direction. The scattering strengths τ_m of the two targets were equal (to unity). As discussed in section 3.2.1 the Coherent Point Spread Function (CPSF) of a regularly spaced antenna array of length a will have an effective lateral width δ at distance z of approximately

$$\delta = z\lambda/a$$

which using $z = 16\lambda$, $a = 4\lambda$ yields $\delta = 4\lambda$. This is equal to twice the spacing between the two targets so this example corresponds to two well-resolved targets. We show in Fig 1 the magnitude of the scattered field $|\psi_j^{(s)}(\mathbf{r}, \omega)|$ for $j = 1, 2, \ldots, 9$ at all points along the x axis (the location of the antenna array) as well as the sample values of this quantity at the array locations (shown with triangles in the figures). We do not display the phase of the scattered field since phase wrapping would prevent a simple comparison of the sampled values of this quantity with the continuously distributed field. The sample values of the scattered field distribution across the antenna array are the values of the MSR matrix $K_{i,j}$ defined in Eq.(34). Thus, the triangles in the j'th image in the figure represent the magnitude of the matrix element $K_{i,j}$, $i = 1, 2, \ldots, N$ and for a specific value of j. This same procedure was employed in all the simulations with the exception that in some cases additive noise was added according to Eq.(33) and we display the noisy sample values relative to the noise free values.

6.0.2 Computing the Eigenvalues and Eigenvectors of the time-reversal matrix

The time-reversal matrix is computed directly from the MSR matrix according to Eq.(8). We used a standard eigenvector/eigenvalue solver in MATLAB to compute the eigenvalues and eigenvectors of the time-reversal matrix in the simulation. Since there are two targets there are two non-zero eigenvalues with associated signal space eigenvectors. We show in Fig. 2 a plot of the eigenvalues and unwrapped phase of the eigenvectors as computed from the MSR matrix whose magnitude is shown in Fig. 1. We see for this case that there are two non-zero eigenvalues corresponding to the two well resolved targets that are separated by eight wavelengths. We also show in the bottom figure the phase of the complex conjugate Green function vectors g_m^* which are seen to be nearly identical (to within an additive integral multiple of 2π) to the phase of the two eigenvectors. This is in agreement with the fact that the complex conjugate of the Green function vectors are proportional to the eigenvectors of the time-reversal matrix in the case of well-resolved targets (cf., 3.2.1). We show only the phase of these quantities since the phase of the field is much more important than amplitude (intensity) in imaging and target location estimation.

6.0.3 Forming the conventional time-reversal image

The time-reversal image is formed using Eq.(24). For the well resolved target case the image field $\psi_m(\mathbf{r})$ is proportional to the Coherent Point Spread Function (CPSF) of the antenna array. This is well approximated in the first simulation where the targets are separated by 8λ. The magnitude of the focused fields from the two eigenvectors for this case (whose phases are shown in Fig. 2) are shown in Fig. 3. We have superimposed an X at the actual target locations to show that the image fields tend to peak in the vicinity of the targets. We have also shown for comparison the magnitude of the fields generated from the complex conjugate Green function vectors g_m^* which are the eigenvectors in the ideal case where the targets are perfectly resolved and whose phase distributions along the antenna elements are also shown in Fig. 2. It is clear from the figure that the image intensities for both the imaged eigenvectors and the imaged Green function vectors are very close as can also be inferred from the fact that their phase distributions along the antenna elements are almost identical as shown in Fig. 2.

It is clear from Fig. 3 that the images generated from the eigenvectors of the time-reversal matrix provide a good indicator of the target locations. The reasons for this are that the targets are well-resolved so that their separate image fields do not overlap significantly. However, we will see later examples where the targets are not well-resolved so that the images generated by the eigenvectors of the time-reversal matrix do not provide good indication of the target locations. Moreover, even in this example where the targets are well separated the depth resolution generated by the classical time-reversal images is not very good. Indeed, a close scrunity of the images in Fig. 3 shows that the maximims do not occur at the target locations but rather in the immediate vicinity of the array (see grayscale bar). The reason for this is at mentioned in section 3.2.1 the longitudinal resolution associated with the CPSF is much less than is the horizontal resolution: a fact that is clear from Fig. 3.

6.0.4 Computing the Pseudo-spectrum

The MUSIC algorithm was implemented using Eq.(26) with the denominator computed using both forms given in Eq.(28). In all of the simulations the two methods of computing the denominator gave essentially equivalent results so we only show the result obtained by the direct method of projecting g_p onto the noise subspace. In the first simulation discussed so far the targets are well-resolved so that each eigenvector is associated with one of the two targets and the conventional method of imaging the eigenvectors illustrated in Fig. 3 gives good indication of target location,

at least as regards the lateral (x) location. The computed pseudo-spectrum for this example is shown in Fig. 4 while Fig. 5 shows the pseudo-spectrum superposed on top of the conventional time-reversal images. Also show in text are the estimates of target location obtained by simply finding the maximum of the pseudo-spectrum. As expected in the absence of noise perfect target location estimation is obtained.

6.1 Further Examples

As a second example we repeated the first simulation but added noise and also increased the spacing between adjacent antenna elements to two wavelengths. In Fig. 6 we plot the magnitude of the scattered field as well as the magnitude of the MSR matrix for a noise standard deviation equal to 20% of the peak value of the magnitude of the (noise free) MSR matrix. The effect of the noise is clear from the plot as is the increased antenna element spacing. In Fig. 7 we show the plot of the eigenvalues as well as the phase of the eigenvectors and complex conjugate Green functions. Note that the noise has the effect of adding non-zero eigenvalues beyond the first two dominant ones. Also note that the phases of the conjugate Green functions are no longer equal to the phases of the first two eigenvectors due to the effect of the increased antenna separation and also the additive noise. In Fig. 8 we show the images generated from the two dominant eigenvectors together with those generated using the complex conjugate Green function vectors. It is seen that these images possess a complicated spatial structure with multiple lobes making it difficult to located the two targets. In Fig. 9 we show the pseudo-spectrum which, although noisy, returns exact estimates of the target locations. The superposition of the pseudo-spectrum with the contour plots of the time-reversal images is shown in Fig. 10 and illustrates that the lobe structure of the time-reversal image makes target location estimation difficult.

To illustrate the effect of antenna element spacing and target separation on the rank of the MSR and time-reversal matrices we show in Fig. 11 plots of the two largest eigenvalues of the time-reversal matrix for two targets, both located at the same depth of sixteen wavelengths, but with target separations of one, two, three and four wavelengths and for antenna element spacing varying from one to twenty wavelengths. The top plots are of the largest eigenvectors and the bottom of the lowest eigenvectors with the dots representing the results for a target separation of one wavelength, the circles for two wavelengths, the crosses for three wavelengths and, finally, the stars represent a target separation of four wavelengths. The horizontal axes represent antenna element separation in number of wavelengths. It is clear from the plots that the rank of the MSR and time-reversal matrix tend to *increase* with target spacing (expected) and antenna element spacing. Indeed, even for a target spacing of a single wavelength the plots indicate that the rank of these matrices will be two if the antenna element spacing is at least four wavelengths.

7 Summary and Future Work

In this paper we have reviewed the theory of time-reversal imaging using multi-static data and merged that theory with the MUSIC method of sub-space signal processing. In particular, it was shown how to employ the *time-reversal matrix* in place of the autocorrelation matrix normally used in MUSIC to generate a *pseudo-spectrum* that yields accurate location estimates of coherent point scatterers from near field multi-static data. The theory was developed for ideal point antennas and point scatterers in arbitrary backgrounds and ignored all multiple scattering between the scatterers. The simulations treated the case of two-dimensional line antennas and line scatterers in a uniform background. All of the material was developed in the frequency domain and the simulations only treated a single frequency component (the monochromatic case) although generalization to multiple frequencies in both the theory and simulations is straightforward. Future work will concentrate on

including the effects of multiple scattering and complex extended objects in the underlying theory and extending the simulations to these more general situations.

A Proof of the Theorem

In this appendix we will prove the theorem presented in section 3 that asserts that for the case of a homogeneous background in three-dimensional space (R^3) with $\Im k > 0$ and for $M \leq N$ targets the rank of the time-reversal matrix is less than the number of targets M if and only if both of the following conditions hold:

1. All of the targets are located on a single plane $\mathcal{P}$ that is orthogonal to at least $N - M + 1$ lines $l_{j,l}$ connecting different antenna elements labeled by indicies j and l,

2. The plane $\mathcal{P}$ is the perpendicular bisector of the $N - M + 1$ lines satisfying condition (1) or all targets on $\mathcal{P}$ are equidistant from every line satisfying condition (1).

As noted in section 3 the time-reversal matrix has the same rank as the MSR matrix K so we will prove the theorem by proving that the MSR matrix K has rank $< M$ if and only if the above two conditions hold.

Since K is, by its definition Eq.(7), a linear sum of outer product matricies formed from the Green function vectors g_m, $m = 1, 2, \ldots, M$, its rank will be equal to the number of these vectors that are linearly independent. In order for two or more of these vectors to be linearly dependent there must exist at least one non-trival solution C to the homogeneous matrix equation $\hat{g}C = \phi$ where $\hat{g}$ is the $N \times M$ matrix whose columns are the Green function vectors g_m:

$$\hat{g} = \begin{bmatrix} G(\mathbf{R}_1, \mathbf{X}_1) & G(\mathbf{R}_1, \mathbf{X}_2) & \ldots & \ldots & G(\mathbf{R}_1, \mathbf{X}_M) \\ G(\mathbf{R}_2, \mathbf{X}_1) & G(\mathbf{R}_2, \mathbf{X}_2) & \ldots & \ldots & G(\mathbf{R}_2, \mathbf{X}_M) \\ \vdots & \vdots & \vdots & \vdots & \vdots \\ G(\mathbf{R}_N, \mathbf{X}_1) & G(\mathbf{R}_N, \mathbf{X}_2) & \ldots & \ldots & G(\mathbf{R}_N, \mathbf{X}_M) \end{bmatrix},$$

and C is an M dimensional column vector and ϕ is the N dimensional null vector. If $M = N$ then this set of equations will have a non-trivial solution and the set $\{g_m\}$ will be linearly dependent if and only if at least two rows of the matrix $\hat{g}$ are linearly dependent. More generally, if $M \leq N$ the set of equations will have a non-trivial solution and the set $\{g_m\}$ will be linearly dependent if and only if at least $N - M + 2$ rows of the matrix $\hat{g}$ are linearly dependent. We will show that the two conditions listed above and in the Theorem are precisely the necessary and sufficient conditions for at least $N - M + 2$ rows of the matrix $\hat{g}$ to be linearly dependent.

The j'th and l'th rows of the matrix $\hat{g}$ will be linearly dependent if and only if

$$G(\mathbf{R}_j, \mathbf{X}_1)G(\mathbf{R}_l, \mathbf{X}_m) = G(\mathbf{R}_l, \mathbf{X}_1)G(\mathbf{R}_j, \mathbf{X}_m) \tag{35}$$

where $\mathbf{R}_j$ and $\mathbf{R}_l$ are the locations of the j'th and l'th antenna elements and $\mathbf{X}_m$ and $\mathbf{X}_1$ are the locations of the m'th and first targets and where the above equation must hold for all m. We limit our attention to a homogeneous background in three-space dimensions so that the Green functions are given by

$$G(\mathbf{R}, \mathbf{X}) = \frac{e^{ik|\mathbf{R}-\mathbf{X}|}}{|\mathbf{R} - \mathbf{X}|} \tag{36}$$

where k is the wavenumber of the background and $R = |\mathbf{R}|$ and $X = |\mathbf{X}|$ denote the lengths of the R^3 vectors $\mathbf{R}$ and $\mathbf{X}$, respectively. We will also assume that the background medium has at least some absorbtion so that $\Im k > 0$. On substituting the above expression for the Green function into

Eq.(35) we then conclude that a necessary and sufficient condition for the j'th and l'th rows to be linearly dependent is that

$$k(d_{j1} + d_{lm}) = k(d_{l1} + d_{jm}) + 2\pi N \quad (37)$$

$$d_{j1}d_{lm} = d_{l1}d_{jm} \quad (38)$$

where

$$d_{jm} = |\mathbf{R}_j - \mathbf{X}_m|,$$

and where N is some integer that depends of j, l, m. If we equate the real and imaginary parts of both sides of Eq.(37) and recall that $\Im k > 0$ we conclude that

$$d_{j1} + d_{lm} = d_{l1} + d_{jm} + \lambda N \quad (39)$$

$$d_{j1} + d_{lm} = d_{l1} + d_{jm} \quad (40)$$

which can both be satisfied only if $N = 0$ and Eq.(40) is satisfied. If we did not have at least some absorbtion in the medium ($\Im k > 0$) then we would have to deal with Eq.(39) rather than Eq.(40) and the subsequent analysis becomes extremely complicated due to the possibility that this equation might possess solutions for values of N other than zero. Thus, in the absense of absorbtion the following analysis only rules out target configurations corresponding to $N = 0$ in Eq.(39) so that other specialized configurations corresponding to $N \neq 0$ may arise that also cause the rank of the MSR matrix to be less than M. In the presence of absorbtion or for the special case of $N = 0$ Eqs.(40) and (38) must both be satisfied for all values of m in order for the j'th and l'th rows of the matrix $\hat{g}$ to be linearly dependent.

If we square each side of Eq.(40) and make use of Eq.(38) we obtain

$$d_{j1}^2 + d_{lm}^2 = d_{l1}^2 + d_{jm}^2. \quad (41)$$

We now make use of the definition of d_{jm} to find that Eq.(41) reduces to

$$|\mathbf{R}_j|^2 + |\mathbf{X}_1|^2 - 2\mathbf{R}_j \cdot \mathbf{X}_1 + |\mathbf{R}_l|^2 + |\mathbf{X}_m|^2 - 2\mathbf{R}_l \cdot \mathbf{X}_m = |\mathbf{R}_l|^2 + |\mathbf{X}_1|^2 - 2\mathbf{R}_l \cdot \mathbf{X}_1 + |\mathbf{R}_j|^2 + |\mathbf{X}_m|^2 - 2\mathbf{R}_j \cdot \mathbf{X}_m$$

which simplifies to yield

$$(\mathbf{R}_j - \mathbf{R}_l) \cdot (\mathbf{X}_m - \mathbf{X}_l) = 0 \quad (42)$$

Eq.(42) states that *all targets must lie in a single plane that is perpendicular to the line joining the j'th and l'th antenna elements.*

Eq.(42) is only a necessary condition since it does not fully incorporate the conditions required by Eqs.(38) and (40). However, it is easily seen that Eq.(42) together with Eq.(38) are equivalent to Eqs.(38) and (40) so that these two equations together constitute necessary and sufficient conditions for the j'th and l'th rows of the matrix $\hat{g}$ to be linearly dependent. To examine the additional requirements imposed by Eq.(38) we select an x, y, z coordinate system where the x axis passes through the two antenna locations $\mathbf{R}_j$ and $\mathbf{R}_l$ so that

$$\mathbf{R}_j = R_j\hat{\mathbf{x}}, \quad \mathbf{R}_l = R_l\hat{\mathbf{x}}$$

where $\hat{\mathbf{x}}$ is a unit vector along the x axis and where R_j and R_l the locations of the antenna elements along this line. We will choose the origin of the x axis so that the x coordinate of $\mathbf{X}_1$ is zero; i.e.,

$$\hat{\mathbf{x}} \cdot \mathbf{X}_1 = 0$$

from which it follows from Eq.(42) that

$$\hat{\mathbf{x}} \cdot \mathbf{X}_m = 0 \quad (43)$$

$\forall m$; i.e., all targets lie in the plane $x = 0$.

Using the above coordinate system we find that Eq.(38) becomes

$$|R_j\hat{\mathbf{x}} - \mathbf{X}_1||R_l\hat{\mathbf{x}} - \mathbf{X}_m| = |R_1\hat{\mathbf{x}} - \mathbf{X}_1||R_j\hat{\mathbf{x}} - \mathbf{X}_m|$$

which, upon making use of Eq.(43) reduces to

$$(R_j^2 - R_l^2)(X_m^2 - X_1^2) = 0 \tag{44}$$

where $X_1 = |\mathbf{X}_1|$, $X_m = |\mathbf{X}_m|$ are the lengths of the $\mathbf{X}_1$ and $\mathbf{X}_m$ vectors. Eq.(44) requires that in addition to all targets being required to lie in a single plane (the plane $x = 0$) that is perpendicular to the line joining the two antenna elements either $|R_j| = |R_l|$ or $X_m = X_1$. If $|R_j| = |R_l|$ the plane $x = 0$ containing all targets must bisect the line joining the two antenna elements while if $X_m = X_1$ all target locations in the plane $x = 0$ must be equidistant from the line connecting the two antenna elements but the exact location of the plane (the origin of the x axis) is arbitrary.

In summary, we have shown that in order for two rows of the matrix $\hat{g}$ to be linearly dependent it is necessary and sufficient that

1. All of the targets are located on a single plane $\mathcal{P}$ that is orthogonal to at least one line $l_{j,l}$ connecting two different antenna elements labeled by indicies j and l,

2. The plane $\mathcal{P}$ is the perpendicular bisector of at least one of the lines satisfying condition (1) or all targets on $\mathcal{P}$ are equidistant from at least one line satisfying condition (1).

If $M = N$ then the above two conditions are necessary and sufficient to guarantee linear dependence of the set of Green function vectors $\hat{g}$. However, if $M < N$ then at least $N - M + 2$ of the rows of the matrix $\hat{g}$ must be linearly dependent in order to guarantee linear dependence of the set $\hat{g}_m$ which then leads to the two conditions stated in the Theorem.

Acknowledgment

The author would like to thank Professors Hanoch Lev Ari of Northeastern University and George Papanicolaou of Stanford University and Mr. Ed. Barile of Witten Technologies for helpful discussions and comments on the material presented in the paper.

References

[1] C. Prada, J.L. Thomas and M. Fink, "The iterative time reversal process: Analysis of the convergence", *Journal of the Acoustical Society of America*, **97**, pp.62-71 (1995).

[2] C. Prada, S. Manneville, D. Spoliansky and M. Fink, "Decomposition of the time reversal operator: Detection and selective focusing on two scatterers", *Journal of the Acoustical Society of America*, **99**, pp.2067-2076 (1996).

[3] R.K. Snieder and J.A. Scales, "Time-reversed imgaing as a diagnostic of wave and particle chaos," *Physical Review E*, **58**, pp.5668-5675 (1998).

[4] N. Mordant,C. Prada, and M. Fink, "Highly resolved detection and selective focusing in a waveguide", *Journal of the Acoustical Society of America*, **105**, pp.2634-2642 (1999).

[5] Charles Therrien, *Discrete Random Signals and Statistical Signal Processing* [Prentice Hall, New Jersey, 1992].

[6] P. Stoica and R. Moses, *Introduction to Spectral Analysis* [Prentice Hall, New Jersey, 1997].

[7] H. Wang and M. Kaveh, "Coherent signal-subspace processing for the detection and estimation of angles of arrival of multiple wide-band sources", *IEEE Trans. Acoustics, Speech and Signal Processing*, **ASSP-33**, pp.823-831 (1985).

[8] H. Hung and M. Kaveh, "Focussing matrices for coherent signal-subspace processing", *IEEE Trans. Acoustics, Speech and Signal Processing*, **36**, pp.1272-1281 (1988).

Figure Captions

Fig.1 Plots of the magnitude square of the scattered field generated across a linear array having nine elements with equal spacing of one-half wavelength together with sample values (diamonds) of the magnitude square of the MSR matrix $|K_{i,j}|^2$, $i = 1, 2, \ldots, 9$. Each separate figure corresponds to excitation by a different antenna element.

Fig.2 (Top) Plot of the magnitude of the eigenvalues of the time-reversal matrix for the simulation parameters used in Fig. 1. (Bottom) plots of the (real) phase of the two eigenvectors corresponding to the two non-zero eigenvalues (solid) and of the phase of the complex conjugate of the two Green function vectors (dashed).

Fig.3 (Left) Images generated by the two eigenvectors shown in Fig. 2 and (right) images generated by the complex conjugate Green function vectors shown in Fig. 2. The "X" on the images indicates the location of the targets.

Fig.4 The pseudo-spectrum computed for the simulation depicted in Figs. 1-3. The peak values of the pseudo-spectrum are given as text in the figure and indicate that exact results were obtained for both the x and z location estimates.

Fig.5 Contour plots of the time-reversal images shown in Fig. 3 on which are superposed the pseudo-spectrums shown in Fig. 4.

Fig.6 Plots of the magnitude square of the scattered field generated across a linear array having nine elements with equal spacing of two wavelengths together with the noisy sample values (diamonds) of the magnitude square of the MSR matrix $|\mathcal{K}_{i,j}|^2$, $i = 1, 2, \ldots, 9$. Each separate figure corresponds to excitation by a different antenna element.

Fig.7 (Top) Plot of the magnitude of the eigenvalues of the time-reversal matrix for the simulation parameters used in Fig. 6. (Bottom) plots of the (real) phase of the two eigenvectors corresponding to the two non-zero eigenvalues (solid) and of the phase of the complex conjugate of the two Green function vectors (dashed).

Fig.8 (Left) Images generated by the two eigenvectors shown in Fig. 7 and (right) images generated by the complex conjugate Green function vectors shown in Fig. 7. The "X" on the images indicates the location of the targets.

Fig.9 The pseudo-spectrum computed for the simulation depicted in Figs. 6-8. The peak values of the pseudo-spectrum are given as text in the figure and indicate that exact results were obtained for both the x and z location estimates.

Fig.10 Contour plots of the time-reversal images shown in Fig. 3 on which are superposed the pseudo-spectrums shown in Fig. 9.

Fig.11 Plots of the eigenvalues of the time-reversal matrix for two targets as a function of antenna element spacing. The top plots are of the largest eigenvectors and the bottom of the lowest eigenvectors with the dots representing the results for a target separation of one wavelength, the circles for two wavelengths, the crosses for three wavelengths and the stars for four wavelengths. The horizontal axes represent antenna element separation in number of wavelengths.

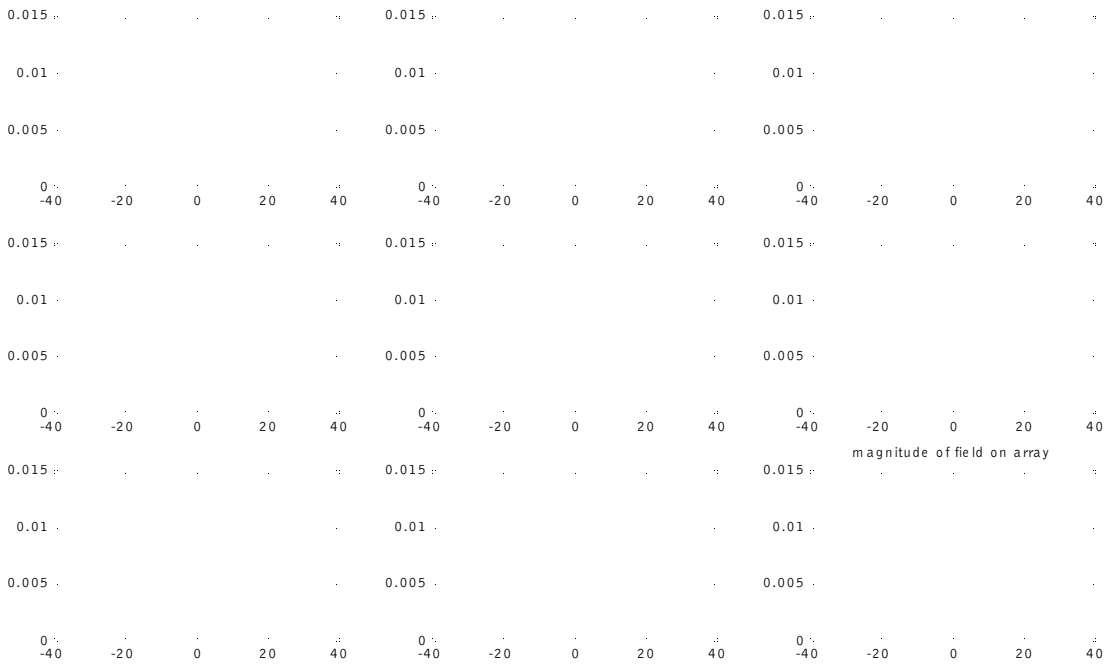

Figure 1:

Figure 2:

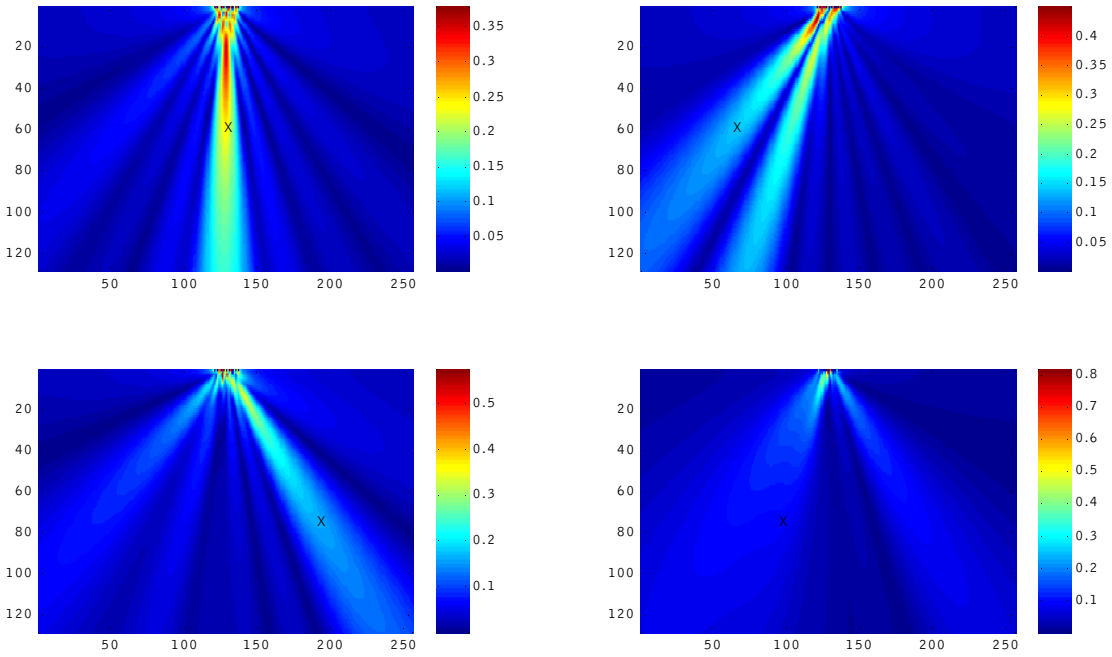

Figure 3:

Figure 4:

Figure 7:

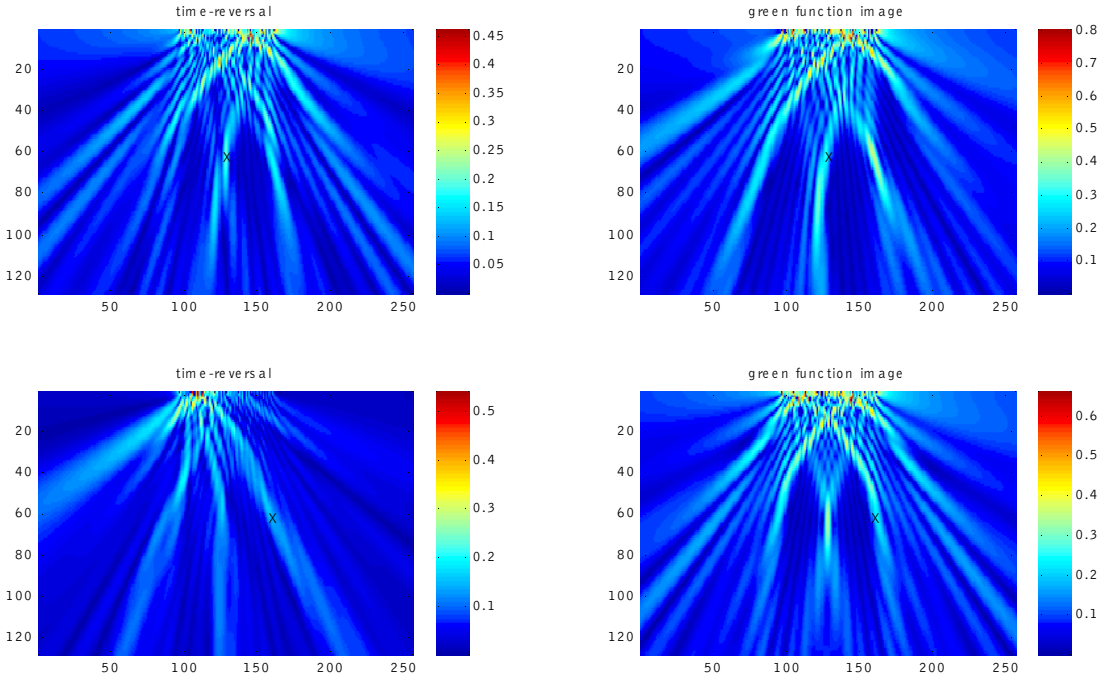

Figure 8:

Figure 9:

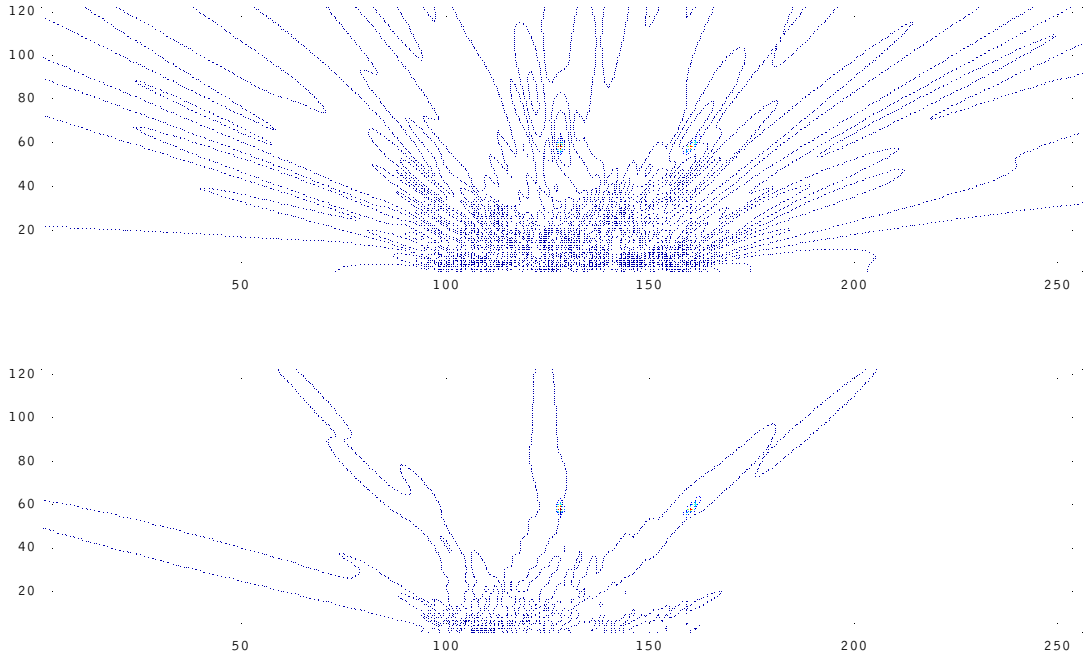

Figure 10:

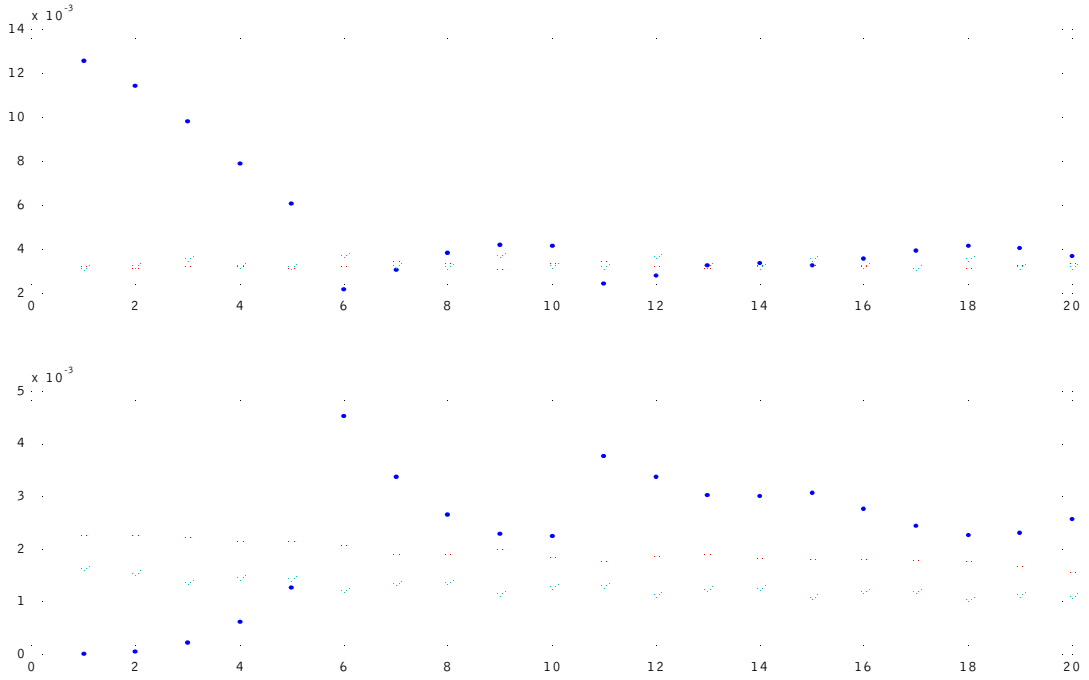
x 10^-3
14
12
10
8
6
4
2
0
2
4
6
8
10
12
14
16
18
20
x 10^-3
5
4
3
2
1
0
0
2
4
6
8
10
12
14
16
18
20

Figure 11: